A simple model for the water retention curve of compressible biocemented sands using MIP results

Rafaela Cardoso[1]*, *Joana* Vieira[2], *Filipa* Calheiros[2] and *Inês* Borges[2,3]

[1]CERIS/IST Instituto Superior Técnico, Universidade de Lisboa, Av Rovisco Pais, 1 1049-001 Lisbon, Portugal
[2]Instituto Superior Técnico, Universidade de Lisboa, Av Rovisco Pais, 1 1049-001 Lisbon, Portugal
[3]INESC-MN, R. Alves Redol, 9 1000-029 Lisbon, Portugal

Abstract. Biocementation treatment consists in using bacteria or other biological agents to promote the precipitation of calcium carbonate (biocement) in the soil pores. When used in slopes for protection against surface erosion, this treatment creates a stiff and strong pervious cover, allowing infiltration necessary to reduce water runoff. The knowledge of the water retention properties of biocemented soils is fundamental knowledge for modelling infiltration but it may not be easy. In this paper the water retention curves of two different treated sands were estimated using a simple model obtained from pores size distribution measured using mercury intrusion porosimetry (MIP) tests. The model proposed considers volume changes of the soil during the MIP test due to the compression of air trapped in the voids. The WRC derived from the MIP tests fits well the points measured using a water dewpoint psychrometer, however it is not possible to check curve fitting below the residual water content due to lack of experimental data.

1 Introduction

Biocementation treatment consists in using bacteria or other biological agents to promote the precipitation of calcium carbonate (biocement) in the soil pores, improving overall mechanical behavior and reducing permeability [1]. The study of the water-retention properties of biocemented soils is scarce [2-4], however it is important to model water infiltration, as it occurs during the treatment and in service conditions. This is particularly important when the treatment is done to provide resistance against erosion of slopes [5].

Studies using MIP data to estimate the WRC were performed for soils with a significant fine fraction. The adjustment is good in general below the air entry value [6], but the curve had to be corrected the entire suction range to consider soil deformation occurring due to soil–water interaction [7,8]. Sandy soils can also experience marked collapse deformations, for example, and therefore there is the possibility to correct the curves from MIP data to consider deformations. The definition of this model explores alternative ways to find information about the WRC when the equipment available is not able to measure low suctions.

The model for the water retention curve presented considers the deformability of the soil during the intrusion, assuming an isotropic elastic behavior, until a minimum void ratio defined by the maximum volume of mercury intruded. It was tested in three different casesm the first two the same poorly graded sand before and after being treated by biocementation, and the third in an uniform graded-size sand after being treated by biocementation.

The water retention curve was measured using WP4 equipment and was adjusted using the model proposed based on pore size distribution from mercury intrusion porosimetry tests, MIP. Complementary information about the two soils is presented, necessary for model calibration.

2 Model proposed

The model proposed is based in the one proposed by Romero et al. [9] for clayey soils. The difference is that the volume changes result from the intrusion process [10], due to the compressibility of the air trapped in the sample voids. Because it is difficult to characterize this differential, it is assumed that the exterior mercury was applying pressure in a material with some compressible air trapped in closed and inaccessible pores. Only the drying path of the WRC was simulated using the intrusion data from pore size distribution.

Suction, s, can be computed directly from mercury pressure, pHg, using the Laplace equation:

$$s = \frac{T_w cos\theta_w}{T_{Hg} cos\theta_{Hg}} p_{Hg} \quad (1)$$

where T_w and T_{Hg} are the surface tensions of water and mercury, respectively (T_w=0.073 N/m and T_{Hg}= 0.489 N/m), and θ_w and θ_{Hg} are the contact angles of water and mercury, respectively (θ_w= 0° and θ_{Hg}= 120°).

* Corresponding author: rafaela.cardoso@tecnico.ulisboa.pt

The degree of saturation, Sr, can be computed by using Equation (2), and the water content can be computed by using Equation (3) [9]:

$$S_r = (1 - S_{rm}) + \frac{w_{res}}{w_{sat}} S_{rm} \quad (2)$$

$$w = (1 - S_{rm})(w_{sat} - w_{res}) + w_{res} \quad (3)$$

In these equations, S_{rm} is the degree of saturation computed considering the volume of mercury intruded until that step, in relation to the maximum volume of intruded mercury (Equation (4)), and w_{res} represents the voids that cannot be filled with mercury (Equation (5)). Both parameters are determined by knowing the void ratio filled with mercury until the current stage, e_{MIP}, which is the volume of mercury intruded divided by the volume of solids of the sample, and the maximum void ratio that was filled in the intrusion phase e_{MIPmax}, which is the maximum volume of mercury intruded divided by the volume of solids of the sample. Parameter w_{res} is updated during the intrusion process to consider changes in the void ratio, Δe (Equation (6)) of the soil when compressed inside the intrusion penetrometer. For this reason, a compressibility index α is adopted to compute the reduction in void ratio during compression caused by increasing mercury pressure, adjusted numerically to consider the compressibility of air bubbles and that of the soil, with or without the presence of biocemented bonds. The water content of the soil when fully saturated is w_{sat} and the void ratio, e, at preparation is determined as usual (Equation (7), where Gs is the density of the solid particles).

$$S_{rm} = \frac{e_{MIP}}{e_{MIP,max}} = \frac{V_{intruded}}{V_{max,intruded}} \quad (4)$$

$$w_{res} = \frac{e - \Delta e - e_{MIP,max}}{G_s} \quad (5)$$

$$\Delta e = -\alpha \Delta ln p_{Hg} \quad (6)$$

$$w_{sat} = \frac{e}{G_s} \quad (7)$$

Finally, it must be ensured that the void ratio computed while considering volume changes must be larger than e_{MIPmax}.

3 Materials and treatment

3.1 Bacteria and feeding solution

The bacteria used, species *Bacillus pasteurii*, are non-pathogenic and common in soils. The composition of the culture medium was 20 g/L yeast extract, 10 g/L of ammonium sulphate and 0.13 M Tris buffer pH 9.0. They were grown at 30°C until reaching approximately 10^8 cells/mL (an optical density measured for 600 nm OD_{600}=1). The feeding solution was prepared with 0.5 M urea and 0.5 M of calcium chloride in 1:10 diluted growth medium, 2.12 g/L of sodium bicarbonate and 10 g/L of ammonium chloride.

3.2 Soils and sample preparation

Two different quarzitic sands were used: Soil 1, a well graded sand (SW), and Soil 2, a poorly graded sand (SP). Their grading size distributions are in Figure 1 and other relevant properties are in Table 1, such as average diameter, percentage of fines (material passing sieve #200) and the relative particle density Gs.

The samples were prepared with the dry volumetric weights γ_d and initial void ratios presented in Table 1. The dry material was poured in oedometric stainless steel rings (7 cm diameter and 2 cm height) to perform oedometer and permeability tests, and slightly tamped.

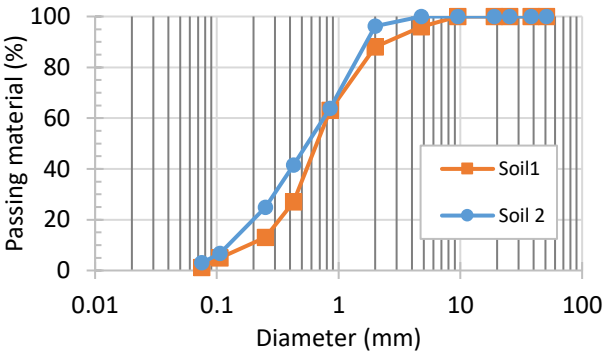

Fig. 1. Grading size distribution curve of the soil.

Table 1. Characteristics of the soils and samples prepared.

	D_{50} (mm)	%Fines	G_s	γ_d (kN/m³)	e
Soil 1	0.65	1	2.61	16.5	0.58
Soil 2	0.55	3	2.70	14.5	0.78

3.3 Biocementation treatment

Two types of samples were prepared. The first were prepared with distilled water without any treatment (untreated), which are the control samples. The second were treated by biocementation.

For the treatment, the samples were placed above a plastic grid, which creates a gap (0.5 cm) between their bottom and that of the reservoir, so that the fluids with bacteria and with feeding solution could flow through the samples (see Figure 2).

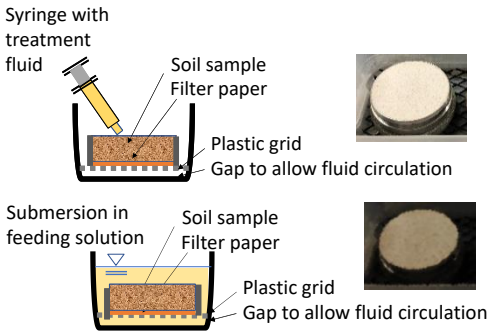

Fig. 2. Treatment protocol (adapted from [4]).

The solutions were added to the soil in the first three days of treatment using a syringe to drop the fluid in the entire surface of the samples. First, the bacteria solution was added to fill one third of void volume V_V ($1/3V_V$).

Then, 10 minutes later the feeding solution was added to fill the other two thirds of void volume ($2/3V_V$). In the next three days, the samples were submerged in the feeding solution. It can be assumed that all the samples were full saturated during and after the treatment.

4 Experimental data available

4.1 Saturated compressibility

The oedometer tests were performed only in full saturated samples, submerged in distilled water independently from being treated or untreated. Full saturation was applied by submersion under the vertical stress of 25 kPa. The loading path was 25, 50, 100, 200, 400, 800, 1200 kPa and the unloading was 400 and 25 kPa. The load increments were applied each 24 hours.

The elastoplastic and elastic compressibility indexes, Cc and Cs, are presented in Table 2 for the samples with and without treatment (Biocem. and Untreat., respectively) of the two soils, as well as the yielding stresses σ'_y.

Table 2. Summary of the experimental data for the two soils.

	Soil 1		Soil 2	
	Untreat.	Biocem.	Untreat.	Biocem.
Cc	0.137	0.162	0.037	0.108
Cs	0.014	0.013	0.011	0.014
σ'_y(kPa)	80	100	48	170
k (m/s)	$5.4x10^{-5}$	$4.1x10^{-5}$	$5.5x10^{-4}$	$2.9x10^{-5}$
CCC	---	3.4%	---	14.3%

For the two soils, the presence of the biocemented bonds increase the values of the yielding stresses σ'_y. The values of Cc found are larger for the biocemented soil than for the untreated one, independently from suction. This result was also found by others [11-13] and can be explained by structure loss caused by bond breakage during the increment of vertical stress. Similar behaviour is also observed in structured soils when progressive bond breakage occurs during loading [14]. The possibility that biocement can be dissolved due to full saturation, if vaterite is precipitated instead of calcite [15], also may explain the behaviour observed.

The elastic compressibility indexes Cs computed for the untreated and treated cases are almost the same. This may indicate that almost structure was lost during loading, probably because the amount of biocement precipitated was small.

4.2 Saturated permeability

The saturated permeability was measured in a permeameter adapted to the size of oedometer samples [16]. The values are presented in Table 2. As expected, the permeability of soil 2 was larger than that of soil 1 because it is a uniform graded size soil.

Permeability decreased slightly after the treatment. This is expected because the amount of biocement precipitated should had some clogging effect of the soil pores [17]. This effect was more marked for Soil 2 than for Soil 1 because a large percentage of calcium carbonate (CCC in Table 2) was found for this soil.

4.3 Water retention curve

The water retention curve was measured using equipment WP4-C [18,19]. This equipment allows suction measurements between 0.5 and 84 MPa, not enough for sandy soils, as their air entry value is below 1 MPa. Only the drying paths are analyzed in this paper, to be compared with the pore distribution curve of the intrusion part of the MIP test. The equation proposed by Van Genuchten [20] (Eq. 8) was used the experimental data because this equation is the one most used in commercial programs.

$$Sr = \left(1 + \left(\frac{s}{P}\right)^{\frac{1}{1-y}}\right)^{-y} \quad (8)$$

In Equation 8, s is suction, Sr is the degree of saturation, P is the air entry value (MPa) and y is a constant. Constants P and y are determined numerically.

The experimental points for the two soils are presented in Figure 3, as well as curve fitting done using Equation 8. The calibration parameters are in Table 3, adjusted to minimize overall error.

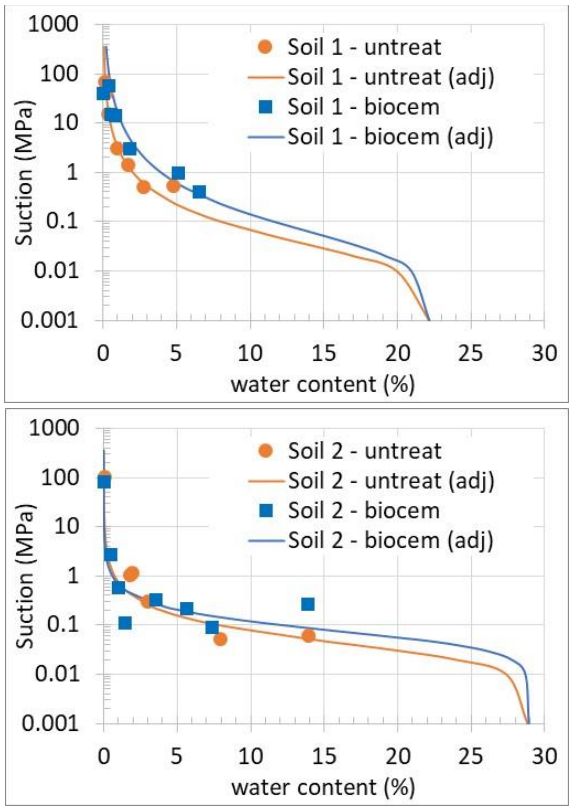

Fig. 3. Water retention curves for: a) Soil 1; b) Soil 2.

Both sandy soils present WRC with a large transition zone, being more marked for Soil 2, the uniform-graded

sand. The differences on the water retention behavior observed before and after the treatment are expected because the pores geometry (size, volume, tortuosity) has changed. For both soils, the air entry value P has increased slightly after the treatment due to pore clogging caused by the presence of the biocement. The increment of this value more marked for Soil 2 because of the largest amount of biocement precipitated (CCC in Table 2).

Table 3. Calibration constants for the water retention curve using Eq. 8.

	Soil 1		Soil 2	
	Untreat.	Biocem.	Untreat.	Biocem.
y	0.38	0.33	0.51	0.58
P (MPa)	0. 02	0.03	0.03	0.06

4.4 Mercury intrusion porosimetry tests

Mercury intrusion porosimetry tests (MIP) were performed in cubic pieces extracted from the samples ($1\times1\times1 cm^3$) after being air-dried at laboratory environment for 48 hours. It was impossible to prepare a sample of untreated Soil 2 for this test. The pore size distribution curves from the MIP tests are presented in Figure 4 for the two soils.

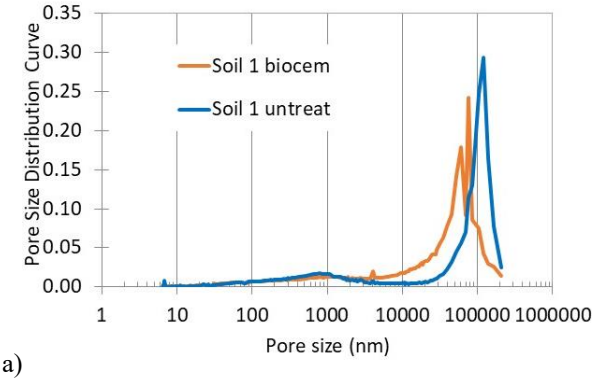

a)

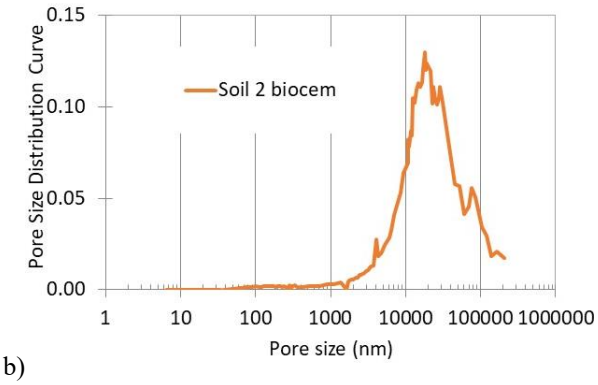

b)

Fig. 4. Pore size distribution curves for: a) Soil 1; b) Soil 2.

Considering first Soil 1, a marked peak is found at 100 µm and a second smaller one around 800 nm for the untreated soil, suggesting a bimodal pore size distribution. This small peak is observed for the biocemented soil as well, while the larger peak found for this soil is composed by two dominant pore sizes: 75 µm and 60 µm. Overall, pore sizes reduce after the biocementation treatment, being this result consistent with the reduction of permeability observed after the treatment (Table 2).

For Soil 2 after the biocementation treatment, a marked peak is measured at 18 µm, with a smallest one at 75 µm. It cannot be considered to have bimodal pore size distribution, however, because there are many pores between these two diameters.

5 WRC from MIP data

The WRC computed from pore size distribution measured in the MIP tests using the model proposed are presented in Figure 5. The calibration constants are in Table 4, adjusted to minimize overall error computed using mean square method. Figure 5 also includes the curves found using Eq. 8 for comparison purposes.

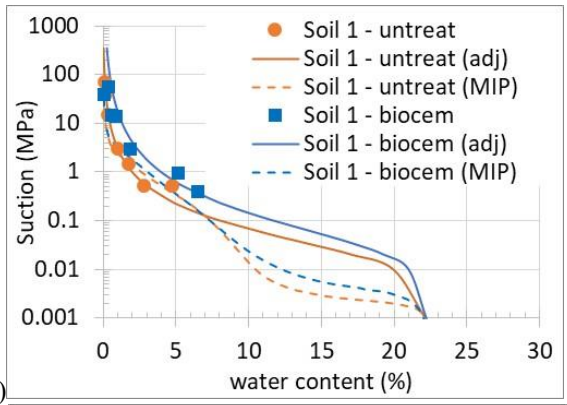

a)

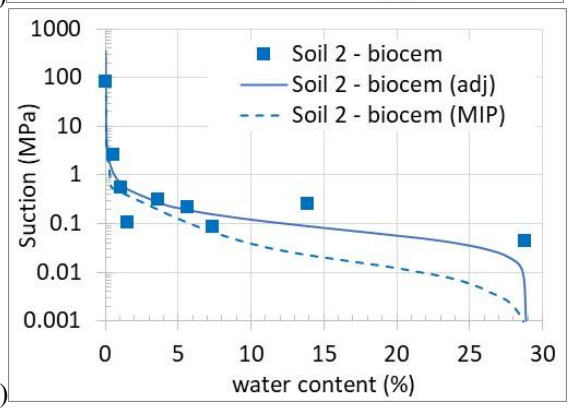

b)

Fig. 5. Water retention curves using the data from the MIP tests and curve fitting using Eq. 8, for: a) Soil 1; b) Soil 2.

Table 4. Calibration constants for the model proposed.

	Soil 1		Soil 2
	Untreat	Biocem	Biocem
α	0.031	0.033	0.078
$e_{MIP,max}$	0.308	0.314	0.264
e	0.582	0.588	0.780
w_{res} (%)	10.5	10.6	19.1

The adjustment found using data from pore size distribution obtained in MIP tests was done considering the experimental points available, which are above

0.5 MPa. These curves are below the curve computed using Eq. 8 below this suction, however there is no experimental data to allow a better calibration of both.

From the shape of the curves, the range of the experimental data is above the residual water content of the soils, as both are sands. For Soil 2 the transition to the lowest suctions above the air entry value is smooth, while one inflection point is observed for both curves of Soil 1. This shape reflects the doble porosity observed for Soil 1 (Fig. 4).

Parameters $e_{MIP,max}$ and w_{res} measured in the MIP test are almost the same for Soil 1 with or without biocementation treatment, probably because the amount of biocement precipitated is not very large (Table 2). Considering only the biocemented samples of the two soils, the intrusion of mercury was more difficult for Soil 2 because w_{res} was larger (and $e_{MIP,max}$ was smaller) for this soil than for Soil 1. This suggests that this soil has more inaccessible pores than Soil 1. This result may be explained by the presence of the biocement, which amount is larger for Soil 2 than for Soil 1.

Parameter α reflects the compressibility of the air trapped in the soil pores. Although being a numerical parameter, the value found for Soil 2 is larger than the one found for Soil 1, which consistent with the smallest $e_{MIP,max}$ and the largest w_{res} measured for Soil 2.

6 Final remarks

A model to find the water retention curve based on pore size distribution from mercury intrusion tests was proposed and tested for two sandy soils. It considers the compressibility of the soil during the porosimetry test, caused by the presence of air entrapped in the soil pores.

The model was calibrated to adjust the experimental points available, all above 0.5 MPa and above the residual water content of the two sands. For clayey soils the adjustment using MIP data is considered acceptable below the air entry value because water adsorbed by clay minerals is not mobilized. No significant amount of water is adsorbed by sand particles and calcite (most usual biocement mineral) so this adjustment also may be acceptable for sands. In addition, these low suctions correspond to small pressures applied, and therefore the uncertainty associated to the compressibility of the air will not affect this adjustment in significant manner.

The model must be tested in other soils with a more complete set of experimental points below 0.5MPa, for example measured with tensiometers or using axis translation technique.

The authors acknowledge Portuguese Foundation for Science and Technology, FCT, I.P, for the funding through projects BIOSOIL ref. PTDC/ECI-EGC/32590/2017, and CALCITE, ref. PTDC/ECI-EGC/1086/2022.

References

1. V. Inanov, J. Chu, V. Stabnikov. Chapter 2 In *Biotechnologies and Biomimetics for Civil Engineering*, F. Pacheco Torgal et al. (eds.) **(**2015).
2. R. Saffari, E. Nikooee, G. Habibagahi, M.T. van Genuchten. *J. Geotech. Geoenv. Eng.,* **145**(7): 04019028. (2019)
3. R. Saffari, E. Nikooee G. Habibagahi. *Proc 4th European Conf Unsaturated Soils*, Eds R. Cardoso, C. Jommi and E. Romero, E3S Web of Conferences, **195**, 05009. (2020)
4. R. Cardoso, J. Vieira, I. Borges, I., *Applied Sciences*, (2022)
5. R. Fernandez, R. Cardoso. *Transportation Geotechnics*, **37**, 100873. (2022)
6. I. Garcia-Bengochea, C.W. Lovell, A.G. Altschaeffl, *J. Geotech.Eng. Div.*, ASCE **105**(7), pp. 839–856. (1979)
7. M. Wang, G.N. Pande, S. Pietruszczak, Z.X. Zeng, *J. Rock Mech. Geotech. Eng.*, **12**, pp. 1356-1360. (2020)
8. R. Hu, Y.F. Chen, H.H. Liu, C.B. Zhou. *Géotechnique*, **63**(16), pp. 1389–1405. (2013)
9. E. Romero, P.H. Simms. *Geotech. Geol. Eng.*, **26**, pp. 705–727. (2008)
10. D. Penumadu, J. Dean. *Can. Geotech. J.* **37**(2), pp. 393–405. (2000)
11. P.H. Simms, E.K. Yanful, *Géotechnique*, **52**(4), pp. 269–278. (2002)
12. R. Harran, D. Terzis, L. Laloui. *J. Geotech. Geoenv. Eng.*, **148**(10), pp. 1-12, 04022074. (2022)
13. R. Cardoso, I. Borges, I. Pires. *Congress on Numerical Methods in Engineerin*g, (2019).
14. M.M. Lee, W.S. Ng, and Y. Tanaka. *Ecol. Eng.*, **60**, pp. 142-149. (2013)
15. S. Leroueil, P. Vaughan. *Géotechnique*, **40**(3), pp. 467-488. (1990)
16. R, Cardoso, R., Pedreira, S.O. Duarte, and G. Monteiro. *Eng. Geo.*, **271**, 105612 (2020)
17. J.T. DeJong, M.B. Fritzges, K. Nusslein. *J. Geotech. Geoenv. Eng.*, **132**: 1381-1392 (2006).
18. A. Al Qabany, K. Soga and C. Santamarina. *J. Geotech and Geoenv Engineering*, **138**: 992-1001. (2012)
19. E.-C. Leong, S. Tripathy and H. Rahardjo. *Géotechnique* **53**(2), pp 173–182. (2003)
20. R. Cardoso, A. Lima, E. Romero, A. Ferrari. *A comparative study of soil suction measurement using two different high-range psychrometers*, in Proc. 2nd Int. Conf. Mechanics of Unsaturated Soils, Germany, Springler (2007)
21. M. T. van Genuchten. Soil Sci. Soc. Am. J. **44**, pp. 892-898. (1980)